

Recent tree-growth reduction in north central China as a combined result of a weakened monsoon and atmospheric oscillations

Shuyuan Kang · Bao Yang · Chun Qin

Received: 16 August 2011 / Accepted: 1 March 2012 / Published online: 3 April 2012
© Springer Science+Business Media B.V. 2012

Abstract Tree-ring records are a valuable source of information for understanding long-term, regional-scale drought changes. In this study, a tree ring width chronology spanning the last 330 years (A.D. 1681–2010) is developed for the northern fringe of the Asian summer monsoon in north central China based on tree ring widths of the Chinese pine (*Pinus tabulaeformis*) at three sites in the Hasi Mountain (HSM). An annual (running from the previous August to the present July) Palmer Drought Severity Index (PDSI) series is reconstructed for the period A.D. 1698 to 2010 using a linear regression model. This reconstruction accounts for 49 % of the actual PDSI variance during the calibration period (A.D.1951–2005). During the last past 330 years, the year 1759 drought was the most severe and the 1926–1932 drought was the most long-lasting. These drought episodes resulted in huge economic losses and severe famine. Similar periods of drought are also found in the Great Bend of the Yellow River region, northeastern Tibetan Plateau and northern China. Our drought reconstruction is consistent with the dry-wet index derived from historical documents for the Great Bend of the Yellow River region for the last three centuries, revealing that our annual PDSI reconstruction reflects broad-scale climate anomalies and represents drought variations in the northern fringe of the Asian summer monsoon. The PDSI reconstruction correlates significantly with sea surface temperature (SST) in the eastern equatorial Pacific Ocean and northern Indian Ocean at an annual timescale, implying that El Niño–Southern Oscillation and the Indian monsoon might be influencing drought variability in the study area. Some extremely dry years of 1707, 1764, 1837, 1854, 1878, 1884, 1926 and 1932 coincided with major El Niño events in historical times. The decadal-scale variability is linked to Pacific Decadal Oscillation (PDO) and SST variations in the Atlantic Ocean. The observed recent tree growth reduction is unusual when viewed from a long-term perspective.

S. Kang · B. Yang (✉) · C. Qin

Key Laboratory of Desert and Desertification, Cold and Arid Regions Environmental and Engineering Research Institute, Chinese Academy of Sciences, 320 Donggang West Rd., Lanzhou, Gansu Province, China 730000
e-mail: yangbao@lzb.ac.cn

1 Introduction

Drought events have significant socio-economic and ecological impacts particularly in arid regions (Easter et al. 2000). Evidence from recent studies indicates that the rising intensity of global warming may lead to droughts occurring more frequently and persisting for longer (Cook et al. 2004; Dai et al. 2004; Trenberth et al. 2004). Precipitation in China varies greatly on both annual and seasonal timescales (Zhang and Lin 1992). In some years, flooding follows heavy rainfall, while in other years the rainfall is insufficient to support agriculture in some regions. As result of its monsoon climate, as well as its topography, China has one of the world's highest rates of drought and flood events. The report of damage in China (1949–1995) reports that, of all the disaster categories listed, droughts lead to the greatest economic loss (Damage Report 1995). Several studies have reconstructed the dryness/wetness indices for eastern China for periods covering the last 530 years. These studies have shown that the dry and wet anomalies appeared initially in northeastern China and have since migrated to affect southern China (Hu and Feng 2001; Qian and Zhu 2001). For example, in 2001, the worst drought since 1990 hit north central China, leaving vast tracts of land parched depriving millions of people and livestock of drinking water (People's Daily, 31 May, 2001). During the 1920s and 1930s in northern China at least 4 million people died because of the famine following the mega-drought (Shanxi Committee of Natural Disasters Annals 2002). In the extreme drought year of 1997, there was no outflow from the Yellow River to the sea for more than 300 days. During this time, approximately 700 km of the lower reaches of the Yellow River ceased to contain water. Meanwhile, the river's major tributaries in its middle reach, including the Fenhe River, Xinhe River, Yihe River, Yanhe River and Weihe River were desiccated.

Therefore, it is extremely important to investigate the characteristics of drought variability and its potential forcing mechanisms at the northern fringe of the Asian summer monsoon in China, and to assess the likely occurrence of similar events in the future. An understanding of drought disasters experienced in the past could help in the evaluation of potential future regional hazards, and also facilitate the assessment of the links between regional and worldwide droughts (Wilhite 2000). Our understanding of drought regimes in this area is limited by the short length of instrumental records. To describe moisture conditions in China, consideration of both precipitation and potential evapotranspiration is important, making PDSI a particularly good indicator of drought (Li et al. 2008). At present, tree rings have been widely used for longer time-scale drought reconstructions (Cook et al. 2010; Esper et al. 2007; Li et al. 2006, 2007). In China, several climate reconstructions of using tree rings have been conducted, for example in the Helan Mountains (Liu et al. 2005a, b) and the Tibetan Plateau (Gou et al. 2008; Shao et al. 2010; Bräuning and Mantwill 2004; Yang et al. 2010a, b), with some records extending back over 1,000 years (Shao et al. 2010).

In this study, we present a drought (PDSI) reconstruction for the Hasi Mountains (hereafter HSM) at the northern fringe of the Asian summer monsoon in central China and discuss the underlying drought regimes, on the basis of a tree-ring width series developed with *Pinus tabulaeformis*. Because the Asian summer monsoon affects moisture conditions over this region, we investigate linkages between drought and atmosphere-ocean circulation of the Indian and Pacific Oceans and Asian monsoon in the HSM region in order to examine the regional climate variability.

2 Materials and methods

2.1 Study area and climate datasets

Our sampling site (Fig. 1, Table 1) is located in the HSM (104°13' to 104°35' E, 36°58' to 37°02' N, 2400–2740 ma.s.l.) in Jingyuan Country, Gansu Province. It is characterized by a semi-arid, continental climate. The HSM formation is mainly a process of the uplift from the eastern part of the fold fault belt on the north side of the Qilian Mountains. The study area lies at the current northern fringe of the Asian summer monsoon, so it may be sensitive to variations in the strength of the atmospheric circulation pattern. The region enjoys a temperate and dry climate with an annual mean temperature in the range 6.0–7.0 °C. Mean annual precipitation ranges from 350 to 400 mm, with the majority of rainfall occurring from July to September. The windy season is mostly from December to February. *Pinus tabulaeformis* are the dominant tree species, growing on north-facing slopes. The study location is located in the transition zone between arid and humid climate (Chinese Committee of Agricultural Resources Planning 1984).

The closest meteorological station, Jingyuan (36.57°N, 104.67°E, 1398 ma.s.l.), provided monthly temperature and precipitation data which were used for the calibration of the tree

Fig. 1 Locations of sampling sites, the meteorological station and PDSI points

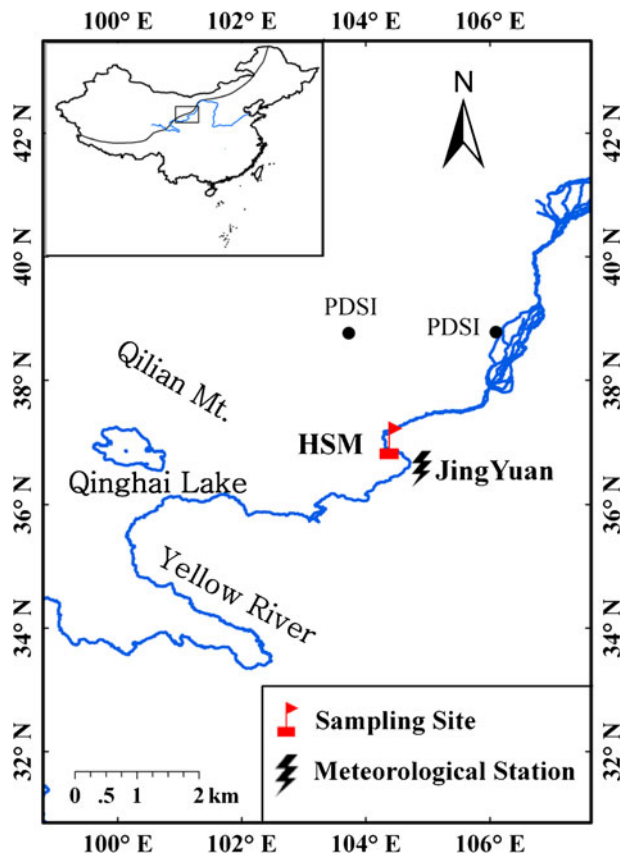


Table 1 Tree-ring sites and instrumental data locations

Site	Latitude	Longitude	Elevation (m)	Core/Tree No.	Period
HSM	37.03°N	104.47°E	2,400–2,740	180/110	1681–2010
JY	36.57°N	104.67°E	1398.2	–	1951–2008
PDSI	38.75°N	103.75°/106.25°E	–	–	1950–2005

HSM, sampling site at Jingyuan County; JY, Jingyuan meteorological station; PDSI, the two closest PDSI grid points from Dai et al. (2004)

growth-climate relationships (Fig. 2). The mean annual temperature was 9.06 °C and the mean annual precipitation was 234 mm for the period 1951–2008 at Jingyuan. There are four Palmer Drought Severity Index (PDSI; Palmer 1965) grid points (Dai et al. 2004) to encompass our sampling sites in HSM. Analysis showed the PDSI values from the two grids south of HSM exhibit a high degree of variability (the largest amplitude), which are very different from the two grids north of HSM. Moreover, the PDSI series from the two PDSI grid points north of HSM show the best agreement among the four PDSI grid points, and had higher correlations with the tree-ring chronology. Taking into account of regional representation and maximum correlation with tree ring chronology, we used two PDSI grid points north of HSM (Fig. 1), which span the period of 1950–2005, to investigate the combined effects of temperature, precipitation and soil moisture on tree growth. The final conclusions are not altered in the case of the inclusion/exclusion of the two PDSI gridded data south of HSM. The gridded monthly PDSI values were derived using monthly temperature (Jones and Moberg 2003; $2.5^{\circ} \times 2.5^{\circ}$ grid) and precipitation data as well as the soil-water holding capacity. The calculation for the PDSI values also takes the precedent condition into account. Precipitation data were obtained from the National Centers for

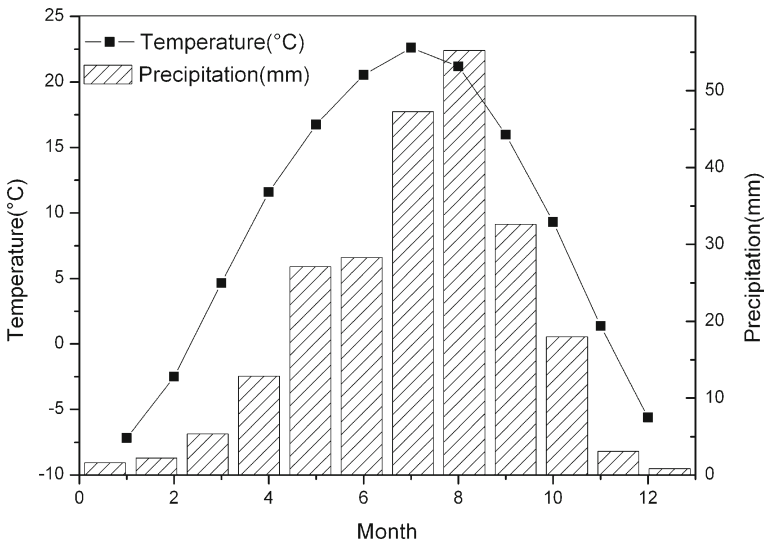


Fig. 2 Mean monthly temperature and precipitation for Jingyuan meteorological station during the period 1951–2008

Environmental Prediction (NCEP) Climate Prediction Center (Chen et al. 2002; Dai et al. 1997). For the soil-water holding capacity, Dai et al. (2004) used a soil texture-based water-holding-capacity map from Webb et al. (1993). The PDSI model also needs some other fixed parameters.

Correlation functions (Fritts 1976) between the tree-ring width and monthly values of temperature and precipitation from the Jingyuan meteorological station were calculated by using the DendroClim 2002 software (Biondi and Waikul 2004). In addition, correlations and response functions between the monthly PDSI dataset (mean of the two PDSI grid series north of HSM) and tree-ring width were also calculated by using the same procedure.

2.2 Tree-ring data and chronology development

In October 2010, a total of 187 cores from 110 living trees were extracted with increment borers at breast height along an altitudinal gradient of 2400–2740 m. All the cores were air dried and mounted on grooved sticks with transverse surfaces facing up (Phipps 1985). Cores were prepared with razor blades to expose ring details to cellular level (Stokes and Smiley 1968). A LINTAB 6 measuring system was used to register ring widths at a resolution of 0.01 mm, and visual inspection facilitated cross-dating of all series (Stokes and Smiley 1968) using the software package TSAP-Win (Rinn 2003). The quality of visual cross-dating was further checked by the COFECHA program (Holmes 1983). These methods ensure the exact dating for each ring-width series. The master series covers the past 330 years from 1681 to 2010, and was constructed from individual series with a mean series length being of 181 years. The mean correlation between single series and the master chronology was 0.67 and the average mean sensitivity was 0.443, confirming the reliable dating of these samples and indicating that tree-ring widths are subject to strong common climatic forcing.

The program ARSTAN (Cook 1985) was used to develop ring width chronologies, and a data-adaptive power transformation was applied prior to standardization in order to remove bias caused by so-called heteroscedasticity (Cook and Peters 1997). There is a biological trend inherent in the raw data series, which is removed by a two-step process. Firstly, an exponential or linear regression curve of any slope was applied to each tree ring-width series. A cubic spline function was then used to detrend the resulting tree ring sequences, subject to a 50 % frequency-response cutoff equal to 67 % of the series length. The residual (or difference) between the transformed ring width measurements and the fitted spline functions were used as tree indices. Tree indices for each year were averaged using the biweight robust mean (Cook and Kairiukstis 1990) to create chronology values. To account for changes in variance attributable to the decline in sample size with time, variance stabilization (Osborn et al. 1997) was applied. The sample size is smaller for the early portion of the tree-ring chronology, and so the expressed population signal (EPS; Wigley et al. 1984) was calculated using a 30-year moving window with 15-year overlaps to assess the reliability of the chronology over time.

The STD chronology from ARSTAN program is the standard version that contains low-frequency information originating from persistent variance of a single tree (Cook 1985). It is computed to enhance the common signal while removing the effects of endogenous stand disturbances. Recent studies indicate that the frequencies retained may be as little as one third of the mean segment length in the chronology (Cook et al. 1995). The mean segment length of our STD chronology is 181 years, and therefore approximately 60 years of variability could be retrieved. The mean sensitivity (MS) was 0.25 for the STD chronology,

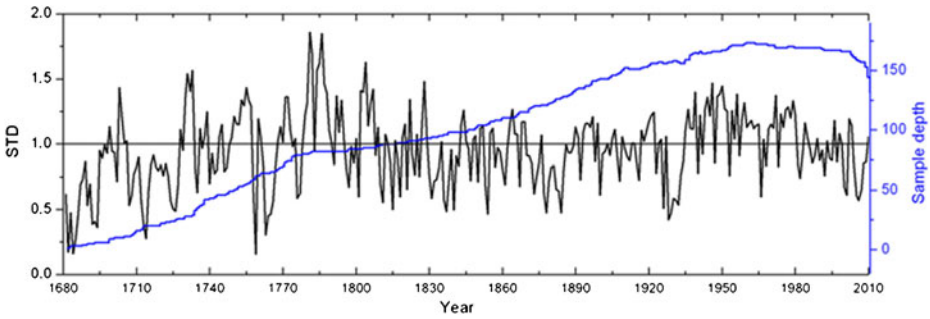


Fig. 3 Standard chronology for HSM (black line) and sample size expressed as number of cores (blue line)

it can be considered to be an indicator of relative changes in the variance of the ring-widths over consecutive years. An assessment of the effects of previous growth is achieved using first-order autocorrelation (AC1), which is 0.54 for the STD chronology (Fritts 1976). As a result, we use the STD version to calculate the response of PDSI to climatic variables in further analysis (Fig. 3). Based on an expressed population signal (EPS) threshold value exceeding 0.85, the most confident period of the standard chronology was from 1698 to 2010 (A.D.).

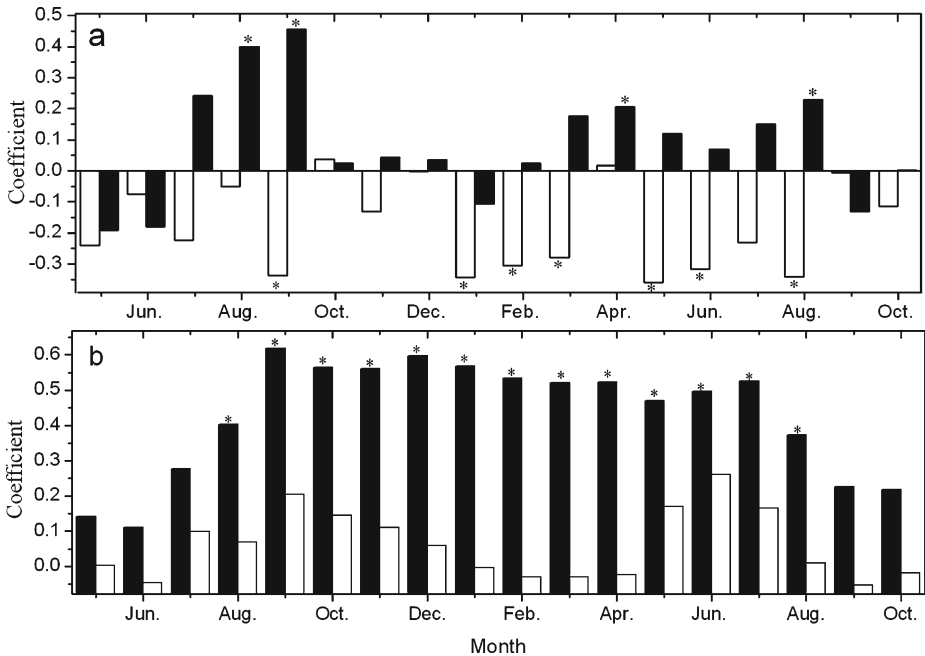


Fig. 4 Correlation and response function analysis of the HSM standard chronology: **a** correlation with temperature (light bars) and with precipitation (solid bars) measured at the Jinyuan meteorological station from 1951 to 2008, and **b** relationship with the mean value of two PDSI grid points from 1951 to 2005, expressed as correlation (solid bars) and response function (light bars). The asterisks indicate significant correlation at 95 % confidence levels

3 Results

3.1 Response to climate variables

Climate-growth analyses were undertaken for the common period 1951–2008 when both tree-ring data and meteorological records were available. As shown in Fig. 4a, significant negative correlations (at the 0.05 level) with temperature were found in September of the previous year ($r=-0.338$), and in January ($r=-0.344$), February ($r=-0.306$), March ($r=-0.280$), May ($r=-0.361$), June ($r=-0.318$) and August ($r=-0.340$) of the current year. By contrast, there was a positive correlation between precipitation during the current growing season and tree growth, this was particularly evident for August ($r=0.229$) of the current year. The other significant correlations with precipitation were found in August ($r=0.401$) and September ($r=0.456$) of the previous year, and April of the current year ($r=0.207$). This positive correlation with precipitation combined with negative correlation with temperature indicates a moisture stressed growth pattern in the drought region (Fritts 1976). Precipitation and temperature are both significant to the modulation of tree growth in the area studied, as both have an effect on soil moisture availability. A further influence on soil water balance is the potential evapotranspiration demand, which is directly modulated by temperature and has been found to correlate strongly with tree growth (LeBlanc and Terrell 2001).

In light of the above analysis, we explored the correlation between ring width and monthly PDSI over their common observation period of 1951–2005, thereby taking both precipitation and temperature into account (Palmer 1965). It was found that tree rings showed stronger correlations with PDSI than with meteorological records (Fig. 4b). At the 95 % confidence level, most of the correlations were significant, except for those in September and October of the current year, and in May–July of the previous year. Peak correlation occurred in September ($r=0.619$) of the previous year. The correlation and response function results indicated that PDSI is the limiting factor for tree growth in the study region. Consistent with other findings in the north central China (Li et al. 2007; Fang et al. 2009), higher correlations were found between tree ring width and PDSI rather than temperature and precipitation.

It is recognized that the PDSI averaged over a single growing month may be less representative of moisture conditions for the growing season than the seasonally averaged PDSI (Cook et al. 1999). We therefore tested several seasonal combinations of PDSI for the purposes of drought reconstruction. The highest correlation between tree ring width and seasonal PDSI was found for the period from August of the previous year to July of the current year ($r=0.7$), which agrees well with the pattern of individual monthly correlations in Fig. 4b. This period was therefore used in the subsequent reconstruction of drought episodes. We also investigated the correlation between ring width and dry-wet index constructed by using instrumental records. Liu et al. (2002, 2005a, b) constructed a dry-wet index (DWI) based on the ratio of temperature to precipitation. Qian and Zhu (2001) defined a dry-wet index $DI = \Delta T / S_T - \Delta P / S_P$, where DI is the dry-wet index; ΔT and ΔP are the anomalies of surface air temperature and precipitation respectively; S_T and S_P are the standard deviations of temperature and precipitation respectively. The highest correlation was found with the DWI ($r=-0.62$) and DI ($r=-0.59$) respectively, averaged from July of the year prior to growth to current June over the instrumental period from 1952 to 2008. These correlations were lower than that with PDSI. Additionally, the PDSI approximates the response of tree growth and the soil moisture reservoir to current and antecedent climatic conditions, and enable direct spatiotemporal comparison of moisture variability for diverse climates and different areas (Dai et al. 2004; Palmer 1965). Therefore, we argued that the PDSI is a more reasonable parameter for climate reconstruction than the dry-wet index derived by observational precipitation and temperature records.

3.2 Regression model and reconstruction

A linear regression model between tree-ring width of HSM and annual PDSI from the previous August to current July (p8-c7) was developed as follows:

$$\text{PDSI}(p8 - c7) = 4.776 * \text{STD} - 5.7237$$

where PDSI is annual PDSI and STD is the tree ring index.

During the calibration period with both ring width and PDSI data (1951–2005), the reconstruction accounted for 49 % of the total PDSI variance (Table 2). As shown in Fig. 5a, our reconstruction successfully captured both the high- and low-frequency variations in local moisture availability. These results are presented notwithstanding the general observation that tree-ring widths tend to provide an under-estimation of the extremes of climate conditions, particularly on the wetter side of the model.

The statistical fidelity of our reconstruction model was evaluated using split-sample calibration-verification and leave-one-out cross-validation methods (Michaelsen 1987) (Table 2). The positive values of reduction error (RE) and coefficient of efficiency (CE) demonstrate that the model yields accurate estimates (Fritts 1976; Cook et al. 1999). CE is more rigorous than RE, and values of CE are normally lower than those of RE indicated good regression model ability (Cook et al. 1999). On the basis of this model, the drought history in HSM region (expressed as conditions from the previous August to current July) was reconstructed for the period A.D. 1698–2010 (Fig. 5b).

4 Discussion

4.1 Drought variability and drought events

Our reconstruction quantitatively extends the drought history for Jingyuan back to 1698, proving a longer background with which to evaluate local moisture variability. Low-frequency variations in PDSI in the HSM were elucidated by applying a 21-year fast Fourier transform (FFT) (Fig. 5b). During the past 300 years, relatively wet years with above-average PDSI occurred in 1760–1812 and 1934–1988, whereas relatively dry years with below-average PDSI prevailed during 1698–1759, 1813–1933 and 1989–2010. The 1810 s–1930s appeared to constitute the most prolonged dry stage.

Table 2 Regression model statistics for different calibration and verification periods

	Calibration (1951–1987)	Verification (1988–2005)	Calibration (1981–2005)	Verification (1951–1980)	Full Calibration (1951–2005)
R	0.67	0.68	0.72	0.57	0.7
R ²	0.45	0.46	0.52	0.33	49 %
R _{adj} ²	0.43	–	0.50	–	–
RE	0.62	–	0.60	–	0.45 ^L
CE	–	0.45	–	0.32	–

R—correlation coefficient; R²—variance explained by the regression model; RE—reduction of error statistic; CE—coefficient of efficiency; L—denotes the leave-one-out verification

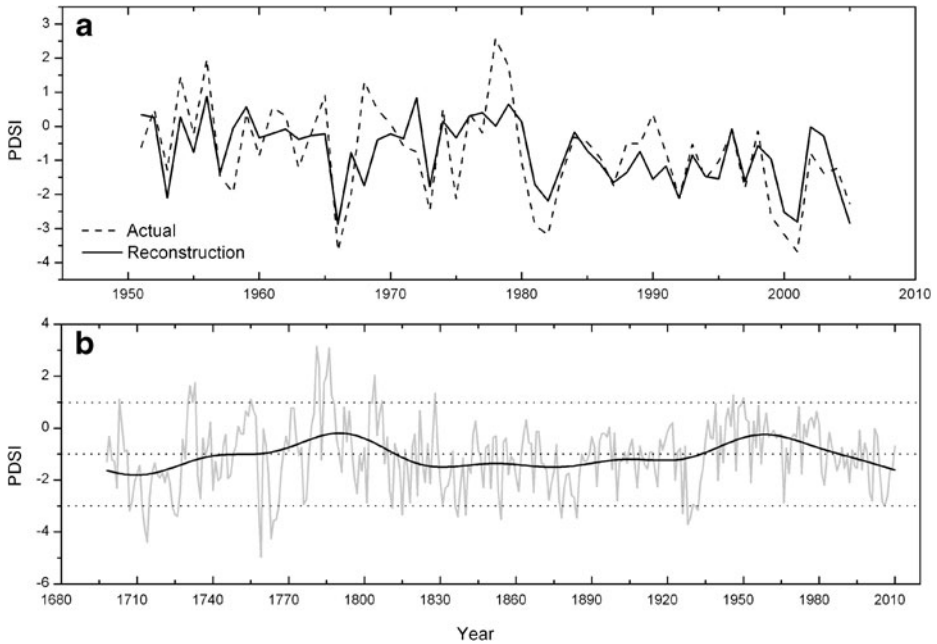


Fig. 5 **a** Reconstructed and observed PDSI during the full calibration period, 1951–2005. **b** The annual (*thin line*) and 21-year FFT (*thick line*) values of the reconstructed PDSI during the period from 1698 to 2010

The mean value of our reconstructed PDSI was -1.08 , which is not within the range of the defined normal moisture status ($\text{PDSI}=0.0\pm 0.5$) (Palmer 1965). The quantitative interpretation of dryness or wetness for a given PDSI value depends on local climatic conditions. For example, in the United States, a PDSI value of $+4$ may imply floods, while the same value would correspond to only moderate rainfall in northern Africa (Dai et al. 2004). In our study, we redefined PDSI values of -1 ± 0.5 to represent normal conditions, and values of less than or equal to -3 or greater than or equal to 1 to represent severe dry or wet conditions (Li et al. 2007), respectively. Based on this new definition we interpret our reconstruction as follows. The extremely dry and wet years ($\text{PDSI} \leq -3$ or ≥ 1) accounted for totals of 7.03 % (22 years) and 5.11 % (16 years), respectively. In Fig. 5b, persistent extremely drought periods were found in the early-1710 s (1713–1714), early-1720 s (1724–1726), mid-1760 s (1763–1766) and late-1920s (1928–1929); persistent extremely wet periods occurred in the 1780 s (1781–1782, 1784–1787). In addition, there are some isolated drought years and wet years: for example, 1707, 1759, 1811, 1815, 1837, 1840, 1854, 1878, 1884, 1926 and 1932 were dry years while 1703, 1731, 1733, 1755, 1802, 1804, 1807, 1828, 1946 and 1950 were wet years.

The extreme wet years appear to be less marked than extreme drought years, which may be because tree-ring widths generally preserve drought conditions better than wet conditions (Fritts 1976). Over the length of our reconstruction, the year 1759 appears to be the most severe drought year, and coincided with a similar dry period that occurred at the northern fringe of the East Asian summer monsoon in China—Great Bend of the Yellow River (hereafter GBYR) area (Qian et al. 2011). Extremely dry conditions in 1713–1714, 1766 and 1728 of our reconstruction coincided with periods of reduced tree-ring growth in the

northeastern Tibetan Plateau (Yang et al. 2010b). Extreme drought periods in the 1720 s were also reported in the nearby northeastern Tibetan Plateau (Li et al. 2008) and north China (Liang et al. 2006). It is noteworthy that the drought epoch from 1926–1932, which was the most long-lasting reconstructed drought in HSM, has been found to extend over a large geographic area by many studies in the surrounding areas (Liang et al. 2006). In addition, the 1920s were reported as a severe drought epoch with high temperature and low precipitation in Northwestern China (Yuan 1984; Liang et al. 2003, 2006; Zhang et al. 2005). The year 1928 was the most recent mega-drought, and was associated with two to three million deaths and the low levels in the Yellow River (Xu et al. 1997). In the GBYR region the most severe drought occurred in 1928–1929 (Qian et al. 2011), which agrees with persistent extremely dry epochs inferred from the HSM. Occurring simultaneously, sustained drought and a plague of locusts, resulted in repeated crop failure, leading to severe famine in northern China from 1927 to 1929; 34 million people suffered and 10 million died as a direct consequence of this event (Deng 1937). In addition, we found that another extreme drought occurred in 1878 in our study area. During the period 1876–1878, thirteen provinces were affected, including Gansu Province in North China (Zhang and Liang 2010). The severity of this drought disaster exceeded even that of the 1928–1930 drought which is considered as the most disastrous event in the 20th century (Zhang and Liang 2010). Comparing the similarities between extreme drought events in the HSM and those in the surrounding regions suggests that a common forcing is associated with drought variations in the GBYR region, the northeastern Tibetan Plateau, north China and our region.

We found that the extremely dry years in 1707, 1764, 1837, 1854, 1878, 1884, 1926 and 1932 of our reconstruction coincided with major El Niño events (Quinn and Neal 1992), of which the years 1878 and 1926 had event strengths and El Niño confidence ratings of ‘very strong’ and 5, respectively. Zhang and Xue’s (1994) study of dry-wet periods and historical El Niño periods from 1500–1990 A.D. in China then showed that the areas deficient in rain were distributed in the Inner Mongolia—Gansu Provinces and the Lower Middle Chang-jiang River during the El Niño years (Zhang and Xue 1994). Our study region lies in Gansu Province near Inner Mongolia and is within the region suffering rainfall deficiency in El Niño years. Therefore, dry years in the HSM may be correlated with El Niño events. Of course, not all of the drought years are necessarily El Niño years, as drought can also be influenced by other factors.

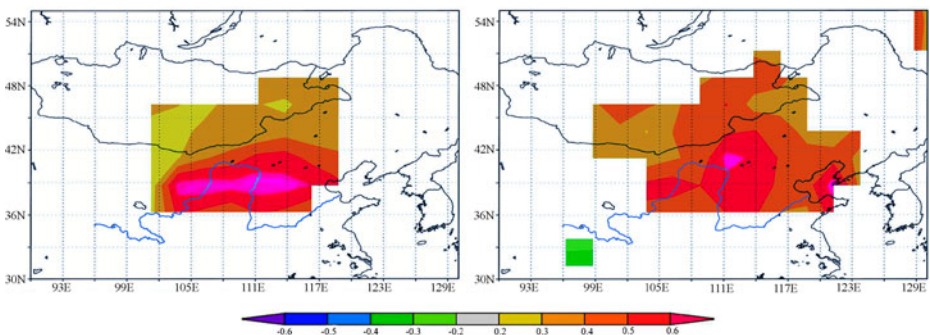


Fig. 6 Spatial correlations of instrumental (*left side*) and reconstructed annual (August to July) PDSI (*right side*) with regional gridded August to July PDSI for the period 1951–2005. The analyses were performed using the KNMI Climate Explorer (Royal Netherlands Meteorological; <http://climexp.knmi.nl>)

4.2 Spatial correlations and comparisons among neighboring areas

To indicate that our drought reconstruction and meteorological records reflected regional-scale PDSI variability, we correlated our reconstruction with the UCAR PDSI available for a user-define region over the calibration period 1951–2005. The analyses were achieved using the KNMI Climate Explorer (Royal Netherlands Meteorological Institute; <http://climexp.knmi.nl>) (Fig. 6). Instrumental records of annual PDSI for the region containing our study area, as well as reconstructed August–July PDSI, were correlated significantly with gridded PDSI on a regional scale. Spatial correlation fields were similar for both reconstructed and instrumental PDSI variability. The highest correlation fields were confined to our study regions. These results demonstrated that our annual PDSI reconstruction captured climatic variations over the wide region at the northern fringe of the Asian summer monsoon in north central China, including a large portion of the GBYR region. A comparison of STD chronology between the HSM and Helan Mountains, which are also located in the GBYR region, suggests that the drought variations between these two regions have been closely correlated over the past three centuries ($r=0.38$, $p=0.01$). For example, droughts during the 1920s to 1930s in our reconstructed series were also identified at the Helan Mountains (Liu et al. 2005a, b) (Fig. 7); the spatially correlated drought variability that exists in this area further suggests that our PDSI reconstruction is representative of a large area.

Yang et al. (2010b) analyzed spatial and temporal growth variations of Qilian Junipers over the northeastern Tibetan Plateau during the period 1450–2001 by applying the

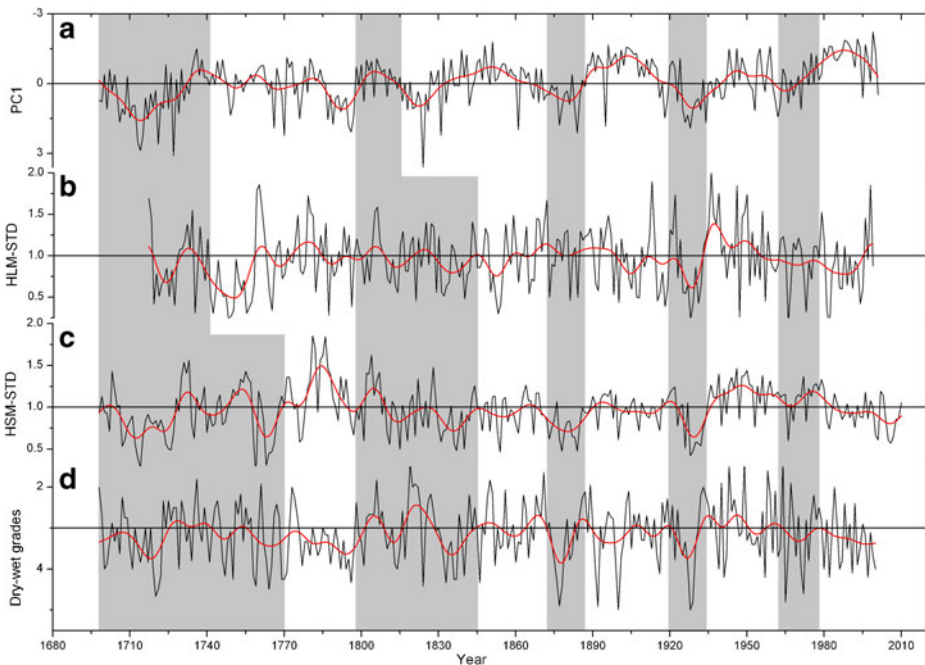


Fig. 7 Comparison of various reconstructions derived from tree-ring records. **a** PC1 of seven moisture-sensitive ring-width chronologies over the Qilian Mountains (PC1, Yang et al. 2010b); **b** Helan Mountains (Li et al. 2007), **c** HSM **d** dry-wet grades in the GBYR region. The black line indicates the annual reconstruction and the red line indicates the 11-year FFT-smoothed values. Common periods are indicated by shaded bars

empirical orthogonal function (EOF) technique to seven moisture-sensitive tree ring-width chronologies, of which the first principal component (PC1) accounts for 51.58 % of the total variance and was adopted as a good indicator of regional precipitation variations on the northeastern Tibetan Plateau. Significant correlation ($r=-0.26$; $p=0.01$, $n=300$) was found between our reconstruction and that of Yang et al. (2010b), probably reflecting long-term similarities between the northeastern Tibetan Plateau and HSM (Fig. 7).

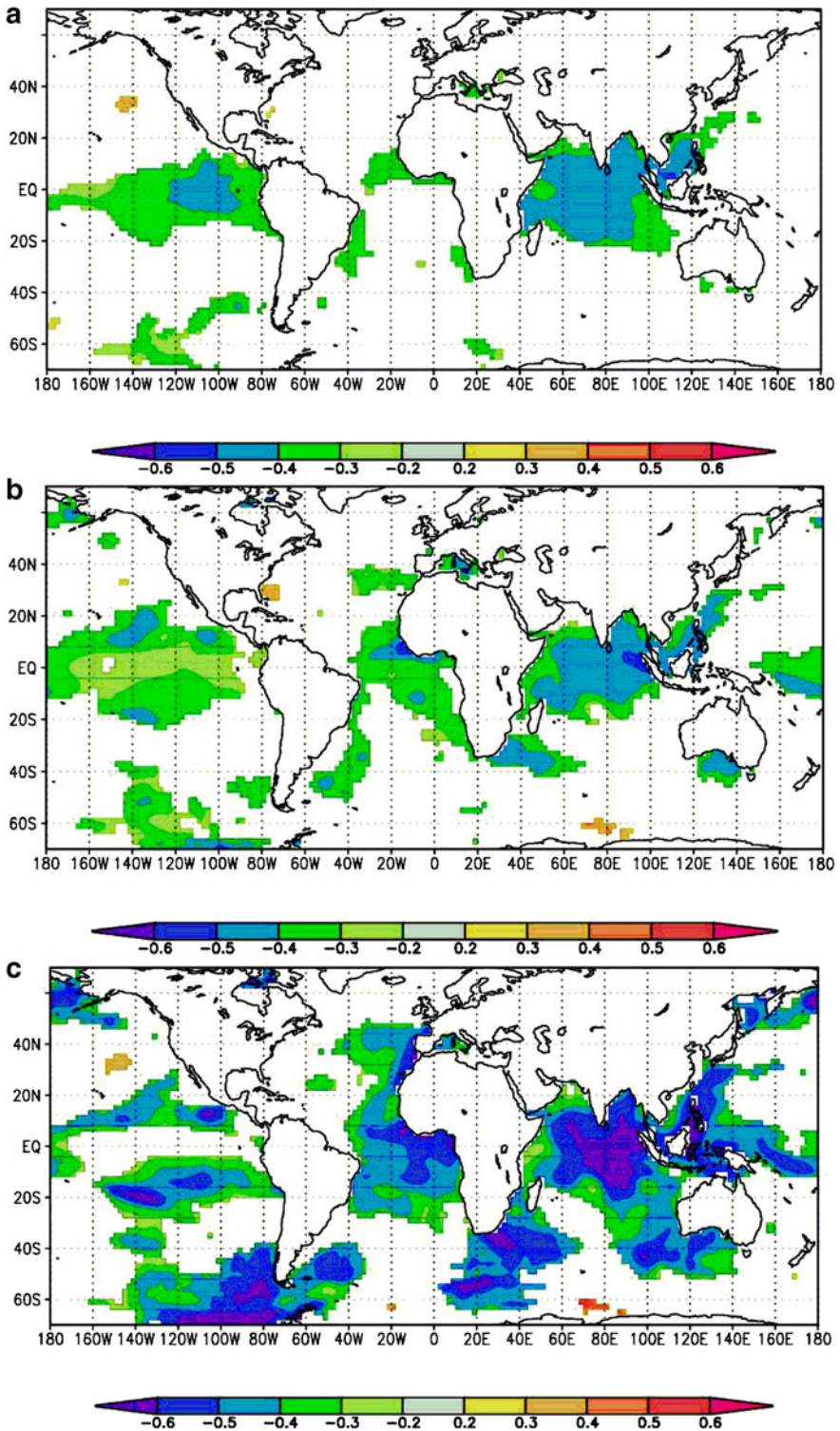
We compared our regional PDSI reconstruction with the gridded PDSI reconstructions by Cook et al. (2010). Their tree-ring network included 327 chronologies for the reconstruction of 534 PDSI points in the domain monsoon Asia, which is strongly exposed to the South Asian summer monsoon. For comparison, the three closest reconstructed PDSI points (36.25°N, 103.75°E; 38.75°N, 103.75°E; 36.25°N, 106.25°E) were extracted from the Cook et al. (2010) dataset for the northern fringe of the Asian summer monsoon in central China. This revealed that patterns of drought variation in the HSM were consistent with the gridded PDSI reconstruction by Cook et al. (2010). In the common period 1698–2005, the correlation coefficient between the present HSM reconstruction and that of Cook et al. (2010) was 0.28 ($p=0.01$). The dry phases during 1830–1850, 1870–1900 and 1920–1940 as identified by the Cook et al. (2010) reconstruction agreed well with our PDSI reconstruction. During these three in-phase periods, the corresponding correlation coefficients were 0.33, 0.44 ($p=0.05$) and 0.62 ($p=0.01$), respectively. These similar variations recorded by both our reconstruction and that of Cook et al. (2010) reflect a common pattern of regional climatic variations during the past three centuries.

Since our reconstruction represents variations in drought intensity at the northern fringe of the Asian summer monsoon in north central China, we compared our results with the dry-wet grade series for the GBYR region during the period from 1680 to 2010 (Fig. 7). The dry-wet grade series was derived by averaging index records of ten sites chosen from 120 dry-wet grade sites. These ten stations provide a good spatial coverage of the GBYR region and exhibit spatial coherence. The dry-wet index was categorized into five grades, namely extremely wet (grade 1), wet (grade 2), normal (grade 3), dry (grade 4), and extremely dry (grade 5). It was found that the drought variabilities of the HSM and GBYR region were reasonably well matched, with a correlation coefficient of -0.25 ($p=0.05$). Therefore, it was concluded that the drought variability of the HSM is representative of the temporal and spatial patterns of the wider GBYR region. Similarly, the dry-wet variability of the GBYR region was found to strongly depend upon whether the southerly monsoon flow can reach northern China (Qian et al. 2011). The sequence of dry-wet years in our study area is therefore discussed with reference to the strength of southerly monsoon.

4.3 Linkages to large-scale atmospheric circulations patterns

The Multi-taper method (MTM) of spectral analysis (Mann and Lees 1996) was used to investigate the variability of local drought in the frequency domain. The analysis was carried out over the full extent of our reconstruction from 1698 to 2010 (Figure omitted). An inter-annual broadband power (at the 95 % level), peaking at 3.4 years, was found for local drought variability. The waveform of the 3 year cycle, as extracted by the MTM method, accounts for 16.8 % of the total variance. We also found other significant peaks at 2.0a, 2.4–2.6a (at the 95 % level) and 5–6a (at the 90 % level). All these significant high-frequency peaks fall within the

Fig. 8 Correlation patterns of the actual, reconstructed and 10-year running mean PDSI with the concurrent NCDC v2 SST over their overlapping periods. **a** Actual Aug-Jul averaged PDSI with concurrent NCDC v2 SST (1951–2004). **b** Reconstructed annual PDSI with concurrent NCDC v2 SST (1951–2004). **c** 10-year running mean of reconstructed annual PDSI with concurrent NCDC v2 SST (1951–2004)



range of El Niño–Southern Oscillation (ENSO) variability (Allan et al. 1996; Sun and Wang 2007), indicating strong teleconnections between drought variability in the HSM and ENSO. This result is consistent with prior studies that have demonstrated the strong effects of ENSO on the variation in rainfall in northern China (Zhang et al. 1999; Feng and Hu 2004) and other areas (Yakir et al. 1996; Schöngart et al. 2004; López et al. 2006; Brien et al. 2010). Some studies have also shown that the Pacific Decadal Oscillation (PDO) has 15–25a and 50–70a cycles (Tourre et al. 2001; Minobe 1997). At the decadal scale, peaks significant at the 90 % level at 12a, 17–18a and 25a have periods close to those of solar activity and the PDO, respectively. Overall, these cycles suggest a strong association between moisture variability in the study area and large-scale ocean–atmosphere–land circulation systems.

In Fig. 8a and b, the significant negative correlations of both the actual and reconstructed HSM PDSI with surface sea temperature (SST) in the equatorial eastern Pacific Ocean and Indian Ocean support a possible connection between drought variability and major moisture source for HSM. When the SST of the middle-east Pacific Ocean and Indian Ocean is low, the West Pacific subtropical high becomes weak and retreats northeastward. Under these conditions, monsoonal China is mainly controlled by the tropical monsoon through, for example, the Intertropical Convergence Zone (ITCZ) (Tan 2009). As a result the moisture flux from the Indian Ocean increases, leading to increasing rainfall intensity in the Chinese monsoon zone. The all-Indian rainfall was significant positively correlated with the HSM tree-ring index ($r=0.351$, $p=0.01$) from 1950 to 2005, which showed that moisture convergence in the HSM is correlated with atmospheric moisture originating from the Indian monsoon. When the temperature of the middle-east Pacific Ocean and Indian Ocean is high, the West Pacific subtropical high becomes strong and subsequently extends southwestward. The moisture flux from the Western Pacific then increases (Tan 2009). These patterns suggest that the variability in HSM rainfall is correlated with variability in the Chinese monsoonal region, reflecting changes in the Indian/Pacific Ocean circulation.

Studies by Fu and Li (1978) and Li and Chen (1979) have shown that when SST in the eastern equatorial Pacific Ocean becomes warmer during El Niño years, the Hadley circulation intensifies. A stronger Hadley circulation will induce a stronger western Pacific subtropical high, which together with a westward shift of the location of the subtropical high can lead to a decrease in the northerly extent of the Indian summer monsoon. This results in reduced precipitation in the semi-arid region of north China. The negative correlation between our reconstructed PDSI and eastern equatorial Pacific Ocean SST from 1951 to 2004 suggests a connection to ENSO. Monsoon dynamics are closely related to ENSO, and influence conditions over much of China (Zhang et al. 1999). Therefore, we concluded that the regional drought variability is possibly related to ENSO and that the region's moisture source may be controlled by the Indian/Pacific Ocean circulation.

We can also see from Fig. 8c that the decadal-scale variability in SST is closely related to the occurrence of drought in the central of north China. The 10-year running mean of PDSI shows significant negative correlation with northern Pacific and Atlantic Ocean SST, suggesting the possible impacts of PDO and NAO on droughts in HSM. The warm phase of the PDO (positive PDO index) corresponds to low precipitation and dry conditions in central North China (Ma 2007). Over the last 55 years, the annual PDO showed a clear shift from a cold to a warm phase during 1976/1977; a shift in precipitation anomaly from positive to negative then followed one year later in 1977/1978 (Ma 2007). Because the intensity of the Asia summer monsoon is closely related to the thermodynamic discrepancy between the East Asian continent and the Pacific

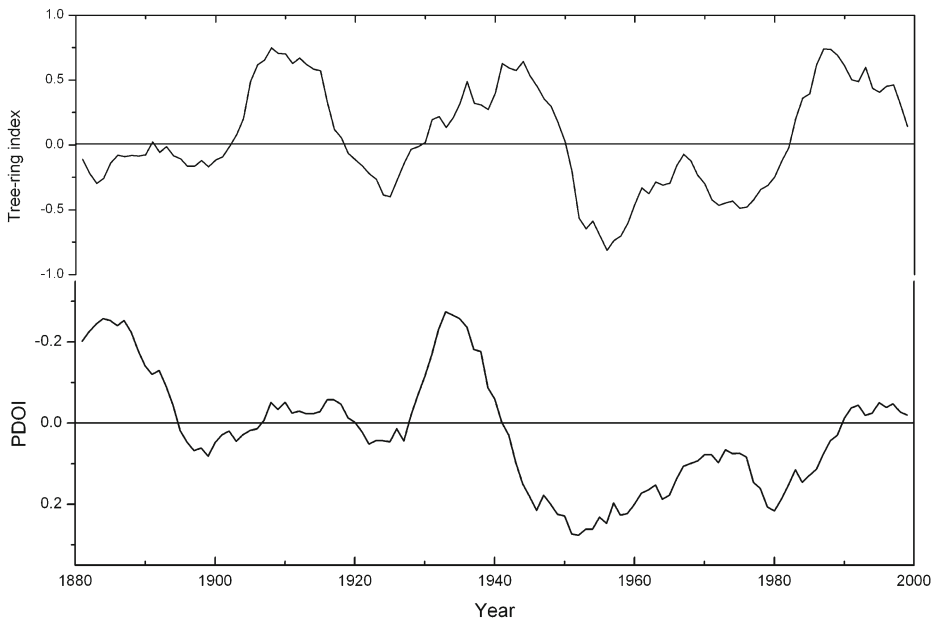


Fig. 9 Variation of 11-year running mean about tree-ring index of HSM (*upper graph*) and PDOI (*lower graph*)

Ocean, the PDO is likely to be the factor controlling the weaker Asian summer monsoon since the mid to late 1970s. In light of these prior studies, we analyzed the relationship between the HSM tree-ring index and 10-year running mean of PDO index (PDOI, <http://jisao.washington.edu/pdo/PDO.latest>) (Fig. 9). We got a significant correlation ($r=-0.33$, $p=0.01$) from 1881 to 2000. We assumed that the PDO is an import factor influencing tree growth in the HSM in north central China. In particular, the reduction in tree growth over the last 50 years is related to the decadal-scale shift in PDO (Fig. 9).

Physical mechanisms controlling fluctuations in the various modes of atmosphere–ocean circulation are still poorly understood, especially for the Asian continent. Nevertheless, while the negative correlation presented in Fig. 9 may be explained by the atmospheric circulation influenced drought variability in this region, the statistical evidence presented above suggests that the drought in our region is related to SST, ENSO, Indian summer monsoon and PDO. Possible forcing mechanisms for regional climate change need further investigation from the perspectives of atmospheric and oceanic circulation systems.

5 Conclusions

A new tree-ring width chronology spanning the period 1681–2010 was established for the northern fringe of the Asian summer monsoon in central China. We used STD index series for reconstruction. Following standard dendroclimatological procedures, an annual PDSI (August–July) series was reconstructed. The reconstruction explained 49 % of the observed PDSI variability for the calibration period 1951–2005. Persistent, extremely dry epochs were identified in the early 1710 s, early 1720 s, mid 1760 s and late 1920s, while persistent, extremely wet periods occurred in the 1780 s (1781–1782, 1784–1787). The severe droughts

in 1878 and the 1920s corresponded to major El Niño events. The PDSI reconstruction in the HSM is representative of the large-scale regional moisture variability at the northern fringe of the Asian summer monsoon in China. Correlation between the reconstructed HSM PDSI and SST in the equatorial eastern Pacific Ocean and Indian Ocean suggests that the regional moisture variability is influenced by linkages with ENSO, the Indian summer monsoon and PDO.

Our results demonstrate the critical importance of further developing large-scale and long-term drought reconstructions over this and surrounding areas, to extend the tree-ring network and enable a more detailed assessment of the spatio-temporal characteristics of extreme drought events. This will allow deeper insights into the atmospheric circulation patterns that influence PDSI patterns over the semi-arid areas at the northern fringe of the Asian monsoon in central China.

Acknowledgments The authors extend many thanks to three anonymous reviewers for their thoughtful comments and suggestions. The study was jointly funded by the Chinese Academy of Sciences (CAS) 100 Talents Project (29082762), the National Basic Research Program of China (973 Program) (No. 2010CB950104), the Chinese Academy of Sciences Visiting Professorship for Senior International Scientists (Grant No. 2009S1-38), and the NSFC (Grant No. 41071130, 41002050).

References

- Allan RJ, Lindesay JA, Parker DE (1996) El Niño Southern Oscillation and climatic variability. CSIRO Publishing, Australia
- Biondi F, Waikul K (2004) DENDROCLIM2002: a C++ program for statistical calibration of climate signals in tree-ring chronologies. *Comput Geosci* 30:303–311
- Bräuning A, Mantwill B (2004) Summer temperature and summer monsoon history on the Tibetan plateau during the last 400 years recorded by tree rings. *Geophys Res Lett* 31:L24205. doi:24210.21029/22004GL020793
- Brienen RJW, Lebrija-trejos E, Zuidema PA, Martínez-Ramos M (2010) Climate-growth analysis for a Mexican dry forest tree shows strong impact of sea surface temperatures and predicts future growth declines. *Global Change Biol* 16:2001–2012
- Chen M, Xie P, Janowiak JE, Arkin PA (2002) Global land precipitation: a 50-yr monthly analysis based on gauge observations. *J Hydrometeorol* 3:249–266
- Chinese Committee of Agricultural Resources Planning (1984) Chinese natural resources planning summary. Science Press, Beijing
- Cook ER (1985) A time-series analysis approach to tree-ring standardization. Ph.D. Dissertation. The University of Arizona Press, Tucson
- Cook ER, Kairiukstis A (1990) Methods of dendrochronology: applications in the environmental sciences. Kluwer Academic Press, Dordrecht
- Cook ER, Peters K (1997) Calculating unbiased tree-ring indices for the study of climatic and environmental change. *Holocene* 7:361–370
- Cook ER, Briffa KR, Meko DM, Graybill DA, Funkhouser G (1995) The ‘segment length curse’ in long tree-ring chronology development for palaeoclimatic studies. *Holocene* 5:229–237
- Cook ER, Meko DM, Stahle DW, Cleaveland MK (1999) Drought reconstructions for the continental United States. *J Clim* 12:1145–1162
- Cook ER, Woodhouse CA, Eakin CM, Meko DM, Stahle DW (2004) Long-term aridity changes in the western United States. *Science* 306:1015–1018
- Cook ER, Anchukaitis KJ, Buckley BM, D’Arrigo RD, Jacoby GC, Wright WE (2010) Asian monsoon failure and megadrought during the last millennium. *Science* 328:486–489
- Dai AG, Funk IY, Del Genio AD (1997) Surface observed global land precipitation variations during 1900–88. *J Clim* 10:2943–2962
- Dai AG, Trenberth KE, Qian T (2004) A global dataset of Palmer Drought Severity Index for 1870–2002: relationship with soil moisture and effects of surface warming. *J Hydrometeorol* 5:1117–1130
- Deng YT (1937) History of famine relief in China. Commercial Press, China, 376

- Easter DR, Evans JL, Groisman PY, Karl KE, Kunkel KE, Ambenje P (2000) Observed variability and trends in extreme climate events: a brief review. *B Am Meteorol Soc* 81:417–425
- Esper J, Frank DC, Büntgen U, Verstege A, Luterbacher J, Xoplaki E (2007) Long-term drought severity variations in Morocco. *Geophys Res Lett* 34. doi:10.1029/2007GL030844
- Fang K, Gou X, Chen F, Yang M, Li J, He M, Zhang Y, Tian Q, Peng J (2009) Drought variations in the eastern part of northwest China over the past two centuries: evidence from tree rings. *Clim Res* 38:129–135
- Feng S, Hu Q (2004) Variations in the teleconnection of ENSO and summer rainfall in northern China: a role of the Indian summer monsoon. *J Clim* 17:4871–4881
- Fritts HC (1976) *Tree rings and climate*. Academic, New York
- Fu C, Li K (1978) The effects of tropical ocean on the western Pacific subtropical high. *Oceanic Selections*, No.2, Ocean Press, 16–21
- Gou X, Chen F, Yang M, Jacoby G, Fang K, Tian Q, Zang Y (2008) Asymmetric variability between maximum and minimum temperatures in Northeastern Tibetan Plateau: evidence from tree rings. *Sci China Ser D: Earth Sci* 51:41–55
- Holmes RL (1983) Computer-assisted quality control in tree-ring dating and measurement. *Tree-Ring Bull* 43:69–95
- Hu Q, Feng S (2001) A southward migration of centennial-scale variations of drought/flood in eastern China and the Western United States. *J Clim* 14:1323–1328
- Jones PD, Moberg A (2003) Hemispheric and large-scale surface air temperature variations: an extensive revision and an update to 2001. *J Clim* 16:206–223
- LeBlanc D, Terrell M (2001) Dendroclimatic analyses using Thornthwaite-Mather-type evapotranspiration models: a bridge between dendroecology and forest simulation models. *Tree-ring Res* 57:55–66
- Li K, Chen Y (1979) Some facts about the effect of the meridional difference of SST anomalies of north Pacific on the subtropical high. *Sci. Atmos Sin*
- Li J, Gou X, Cook ER, Chen F (2006) Tree-ring based drought reconstruction for the central Tien Shan area, Northwest China. *Geophys Res Lett* 33:L07715, 1–5
- Li J, Chen F, Cook ER, Gou X, Zhang Y (2007) Drought reconstruction for north central China from tree rings: the value of the Palmer drought severity index. *Int J Climatol* 27:903–909
- Li J, Cook ER, D'Arrigo R, Chen F, Gou X, Peng J, Huang J (2008) Common tree growth anomalies over the northeastern Tibetan Plateau during the last six centuries: implications for regional moisture change. *Glob Change Biol* 14:2096–2107
- Liang E, Shao X, Kong Z, Lin J (2003) The extreme drought in the 1920s and its effect on tree growth deduced from tree ring analysis: a case study in North China. *Ann For Sci* 60:145–152
- Liang E, Liu X, Yuan Y, Qin N, Fang X, Huang L, Zhu H, Wang L, Shao X (2006) The 1920s drought reconstructed by tree rings and historical documents in the semi-arid and arid areas of northern China. *Clim Change* 79:403–432
- Liu HB, Shao XM, Huang L (2002) Reconstruction of early-summer drought indices in mid-north region of China after 1500 using tree ring chronologies. *Quat Sci* 22:220–229 (in Chinese with English abstract)
- Liu Y, Cai Q, Shi J (2005a) Seasonal precipitation in the south-central Helan Mountain region, China, reconstructed from tree-ring width for the past 224 years. *Can J Forest Res* 35:2403–2412
- Liu Y, Wang L, Shi JF, Cai QF (2005b) Reconstruction of mean drought index from June to August for the last 270 years using tree-ring date in the northern Helan mountain. *Quat Sci* 25:540–544 (in Chinese with English abstract)
- López BC, Rodríguez R, Gracia CA, Sabaté S (2006) Climatic signals in growth and its relation to ENSO events of two *Prosopis* species following a latitudinal gradient in South America. *Glob Change Biol* 12:897–906
- Ma Z (2007) The interdecadal trend and shift of dry/wet over the central part of North China and their relationship to the Pacific Decadal Oscillation (PDO). *Chin Sci Bull* 52:2130–2139
- Mann ME, Lees J (1996) Robust estimation of background noise and signal detection in climatic time series. *Clim Change* 33:409–445
- Michaelsen J (1987) Cross-validation in statistical climate forecast models. *J Clim Appl Meteorol* 26:1589–1600
- Minobe S (1997) A 50–70 year climate oscillation over the North Pacific and North America. *Geophys Res Lett* 24:683–686
- Osborn TJ, Briffa KR, Jones PD (1997) Adjusting variance for sample-size in tree-ring chronologies and other regional mean time series. *Dendrochronologia* 15:89–99
- Palmer WC (1965) *Meteorological drought US*. Weather Bureau Research Paper 45, Washington, DC, 58 pp
- Phipps RL (1985) *Collecting, preparing, crossdating, and measuring tree increment cores*. U.S. Geological Survey Water-Resources Investigations Report, 85–4148
- Qian WH, Zhu YF (2001) Climate change in China from 1880 to 1998 and its impact on the environmental condition. *Clim Change* 50:419–444

- Qian W, Shan X, Chen D (2011) Droughts near the northern fringe of the East Asian summer monsoon in China during 1740–2003. *Clim Change*. doi:10.1007/s10584-011-0096-7
- Quinn WH, Neal VT (1992) The historical record of El Niño events. In: Bradley RS, Jones PD (eds) *Climate since 1500 AD*. Routledge, London, pp 623–648
- Report D (1995) Report of the damage caused by disaster in China. China Statistical Press, Beijing, pp 1–406
- Rinn F (2003) TSAP-Win: time series analysis and presentation for dendrochronology and related applications. Version 0.55 User reference. Heidelberg, Germany (<http://www.rimatech.com>)
- Schöngart J, Junk WJ, Piedade MTF, Ayres JM, Hüttermann A, Worbes M (2004) Teleconnection between tree growth in the Amazonian floodplains and the El Niño–Southern Oscillation effect. *Glob Change Biol* 10:683–692
- Shanxi Committee of Natural Disasters Annals (2002) Historical natural disasters annals. Chinese Meteorological Press, Beijing
- Shao XM, Xu Y, Yin Z, Liang EY, Zhu H, Wang S (2010) Climatic implications of a 3585-year tree-ring chronology from the northeastern Qinghai-Tibetan Plateau. *Quat Sci Rev* 29:2111–2122
- Stokes MA, Smiley TL (1968) An introduction to tree-ring dating. The University of Chicago Press, Chicago
- Sun M, Wang H (2007) Relationship and its instability of ENSO—Chinese variations in droughts and wet spells. *Sci China Ser D: Earth Sci* 50:145–152
- Tan M (2009) Circulation effect: climatic significance of the short term variability of the oxygen isotopes in stalagmites from monsoonal China—dialogue between paleoclimate records and modern climate research. *Quat sciences* 29:851–862
- Tourre YM, Rajagopalan B, Kushnir Y (2001) Patterns of coherent decadal and interdecadal climate signals in the Pacific Basin during the 20th Century. *Geophys Res Lett* 28:2069–2072
- Trenberth KE, Overpeck JT, Solomon S (2004) Exploring drought and its implications for the future. *Eos, Trans-Am Geophys Union* 85:27–29
- Webb RS, Rosenzweig CE, Levine ER (1993) Specifying land surface characteristics in general circulation models: soil profile data set and derived water-holding capacities. *Global Biogeochem Cycles* 7:97–108
- Wigley T, Briffa KR, Jones PD (1984) On the average value of correlated time series, with applications in dendroclimatology and hydrometeorology. *J Appl Meteorol* 23:201–213
- Wilhite DA (2000) Drought: a global assessment. *Natural Hazards and Disasters Series*, Routledge, 700 p
- Xu G, Yao H, Li X (1997) Climate change in arid and semi-arid regions of China. China Meteorological Press, Beijing
- Yakir D, Lev-Yadun S, Zangvil A (1996) El Niño and tree growth near Jerusalem over the last 20 years. *Global Change Biol* 2:97–101. doi:10.1111/j.1365-2486.1996.tb00054
- Yang B, Qin C, Bräuning A, Burchardt I, Liu J (2010a) Rainfall history for the Hexi Corridor in the arid northwest China during the past 620 years derived from tree rings. *Int J Climatol* 31:1166–1176. doi:10.1002/joc.2143
- Yang B, Qin C, Huang K, Fan Z, Liu J (2010b) Spatial and temporal patterns of variations in tree growth over the northeastern Tibetan Plateau during the period AD 1450–2001. *Holocene* 20:1235–1245. doi:10.1177/0959683610371997
- Yuan L (1984) The Northwestern Drought and History of the Famine (in Chinese). The People's Publishing company of Gansu province
- Zhang D, Liang Y (2010) A long lasting and extensive drought event over China during 1876–1878. *Adv Clim Chang Res* 6:106–112
- Zhang J, Lin Z (1992) *Climate of China*. Wiley, New York, 376 p
- Zhang D, Xue Z (1994) Relationship between the El Niño and precipitation patterns in China since 1500 AD. *Q J Appl Meteorol* 5:168–175
- Zhang R, Sumi A, Kimoto M (1999) A diagnostic study of the impact of El Niño on the precipitation in China. *Adv Atmos Sci* 16:229–241
- Zhang Y, Gou X, Hu W, Peng J, Liu P (2005) The drought events recorded in tree ring width in Helan Mountain over past 100 years. *Acta Ecol Sin* 25:2121–2125